이학석사 학위논문

Investigating the Effect of Galaxy Interaction on the Evolution of Spin Alignments

은하 간 상호작용이 은하 스핀 정렬의 진화에 주는 효과 연구

2017년 6월

서울대학교 대학원

물리·천문학부 천문학 전공

구 한 울

Investigating the Effect of Galaxy Interaction on the Evolution of Spin Alignments

A thesis submitted in partial fulfillment of the final requirement for the degree of

Master of Science

Astronomy Program

Department of Physics and Astronomy

Seoul National University

Candidate: **Hanwool Koo**

Supervisor: **Jounghun Lee**

June 2017

Abstract

An observational evidence for the intrinsic galaxy alignments in isolated spiral pairs is presented. From the catalog of the galaxy groups identified by Tempel et al. in the flux limited galaxy sample of the Sloan Digital Sky Survey Data Release 10, we select those groups consisting only of two spiral galaxies as isolated spiral pairs and investigate if and how strongly the spin axes of their two spiral members are aligned with each other. We detect a 4σ signal of intrinsic spin alignment in the isolated spiral pairs, which leads to the rejection of the null hypothesis at the 99.999% confidence level via the Kolmogorov-Smirnov test. It is also found that those isolated pairs comprising two early-type spiral galaxies exhibit the strongest signal of intrinsic spin alignment while the weakest signal is found from the isolated pairs with two late-type spiral galaxies. We also show that the strength of the alignment signal has a weak dependence on the angular separation distance as well as on the luminosity ratio of the member galaxies. Using the dark matter halos consisting of only two subhalos resolved in the EAGLE hydrodynamic simulations, we repeat the same analysis but fail to find any alignment tendency between the spin angular momentum vectors of the stellar components of the subhalos, which is in tension with the observational result. A couple of possible sources of this newly discovered local anomaly is discussed.

Keywords: cosmology:theory — large-scale structure of universe

Student Number: 2014 − 21385

Contents

Chapter 1

Introduction

[1]In the conventional cosmology which aims to track down the expansion and growth history of the whole universe (Linder 2005), it is generally believed that the deeper we look into the past of the universe, the more cosmological information we would obtain about the universe. Quite true as this belief may be, the conventional cosmology is inevitably hindered by unknown (but likely existent) systematics involved with the observations of distant objects. For instance, it has been recently warned that the luminosity-distance relation of the distant type Ia supernovae (SNIa) which is regarded as the first direct evidence for the cosmic acceleration (Riess et al. 1998; Perlmutter et al. 1999) may be substantially contaminated by the systematics involved in the conversion of the brightness of SNIa into its intrinsic luminosity (Nielsen et al. 2016).

For the past two decades, we have witnessed the emergence of a "near-field cosmology", which utilizes the physical properties of the local objects as a test statistics (Bland-Hawthorn & Peebles 2006). Although the evolution history of the universe cannot be traced by observing the local objects, it was realized that the initial conditions of the universe may be imprinted as fossil records in the local objects and thus can

[1]This master thesis written in collaboration with my advisor, Prof. Jounghun Lee, was also submitted as a journal paper for publication in the Astrophysical Journal (ApJ) for an outside review and posted in the preprint arXiv (arXiv:1707.03549). When it is published in ApJ, the copyright of this thesis will be owned by the American Astronomical Society (AAS).

be inferred through careful analyses of the physical properties of the nearby objects (Bland-Hawthorn & Peebles 2006). The obvious merit of using the near-field diagnostics is nothing but relatively low uncertainties in the observations of the local objects, which will allow us to uncover the imprinted (and likely vagnant) fossil records left from the early universe. Furthermore, the near-field statistics will help us undertake a delicately difficult mission of discriminating viable alternative cosmologies from the standard ΛCDM model where the cosmological constant Λ fuels the cosmic acceleration and the most dominant matter content is cold dark matter (CDM).

A variety of near-field diagnostics has so far been developed, which includes the environmental link of the dynamic-to-lensing mass ratio of galaxy clusters, turn-around radii of the galaxy groups, emptiness of cosmic voids, dynamics of the Local Group, correlations of the galaxy peculiar velocities, luminosity-to-mass ratio of isolated dwarf galaxies and so forth (Zhao et al. 2011; Pavlidou & Tomaras 2014; Adermann et al. 2017; Carlesi et al. 2017; Huterer et al. 2017; Peebles 2017, and references therein). The intrinsic spin alignments in the galactic pairs is one of those near-field diagnostics suggested by Lee (2012) who claimed that it would be useful not only to test the standard ΛCDM cosmology but also to distinguish between different coupled dark energy (cDE) models in which the scalar field dark energy is coupled to dark matter particles (for a review Amendola & Tsujikawa 2010, and references therein).

Analyzing the isolated halos consisting of only two subhalos from the adiabatic hydrodynamic simulations (H-CoDECS) that were runfor the cDE models as well as for the ΛCDM cosmology (Baldi et al. 2010; Baldi 2012), Lee (2012) explored whether or not the directions of the three dimensional (3D) spin vectors of two subhalos are aligned with each other and found that some CDE models produced a statistically significant signal of spin alignments in the isolated subhalo pairs while the ΛCDM case yielded no signal. Noting that the strength of the spin alignment in the isolated subhalo pairs depends on the strength of the DE-DM coupling as well as on the shapes of the

DE potentials, Lee (2012) suggested that the spin alignments in the isolated galactic pairs could provide a powerful local diagnostics to test the dark sector coupling.

As mentioned in Lee (2012), however, in order to verify the practical usefulness of this new local diagnostics, two additional tasks must be performed. The first task is to make a theoretical prediction based on a fully hydrodynamical simulation that is capable of resolving luminous galaxies. What Lee (2012) measured is the alignments of the spin axes not of the luminous galaxies but of the DM subhalos resolved in the H-CoDECS which was not capable of simulating the formations of stars and galaxies (Baldi 2012). Given the previous works which have revealed that the spin axes of the luminous galaxies are not necessarily aligned with those of their underlying DM particles (e.g., Hahn et al. 2010; Tenneti et al. 2017; Zjupa & Springel 2017), the numerical result of Lee (2012) cannot be directly compared with those from the observations.

The second task is to improve the observational analyses. Although several works already investigated the spin alignments of the isolated galactic pairs (e.g., Gott & Thuan 1978; Sharp et al. 1979; Helou 1984; Oosterloo 1993; Pestaña & Cabrera 2004; Cervantes-Sodi et al. 2010; Lee 2012), it is still inconclusive whether the intrinsic signals truly exist or not. The main reason for having failed to confirm or to refute convincingly the existence of the spin alignments in the isolated galactic pairs is the poor approximations that the previous works relied on for their analyses. For instance, Cervantes-Sodi et al. (2010) approximated the alignment angles between the spin axes of the member galaxies by the differences in their position angles without attempting to measure directly the 3D spin vectors.

Besides, in the previous works, an isolated galaxy pair was selected not as a bound system composed of two galaxies without being embedded in a larger structure but just as two galaxies closely located with each other. But, recall that the mechanism which generates the alignments between the spin axes of the closely located neighbor galaxies is different from that responsible for the alignments in the isolated galaxy pairs. While

the former is usually ascribed to the combined effects of the spatial correlations of the surrounding tidal field (Peebles 1969; Doroshkevich 1970; White 1984; Dubinski 1992; Barnes & Efstathiou 1987; Catelan & Theuns 1996; Lee & Pen 2000, 2001; Porciani et al. 2002) and the filamentary merging along the cosmic web (Codis et al. 2012), the latter is believed to be generated by nonlinear galaxy-galaxy interaction (Gott & Thuan 1978; Helou 1984). It should be necessary to sort out properly isolated galaxy pairs that forms a bound system, to properly measure the alignment angles directly from the 3D spin axes, and then to employ a robust statistical test of the null hypothesis of no alignment.

Here, we intend to perform the above two tasks. The main contents of the next three chapters can be summarized as follows. In Chapter 2, we present an observational evidence for the existence of the intrinsic spin alignments in the isolated spiral pairs. In Chapter 3, we show that the numerical analysis based on a full hydrodynamical simulations fails to detect any signal of intrinsic spin alignment in the isolated pair system. In Chpater 4, we discuss possible origins of the inconsistencies between the numerical and the observational results.

Chapter 2

An Observational Signal of Intrinsic Spin Alignments in the Isolated Pairs

Tempel et al. (2014) identified the galaxy groups by applying a modified friends-of-friends (FoF) group-finding algorithm to a flux limited sample of the galaxies from the tenth data release of the Sloan Digital Sky (SDSS DR10 Ahn et al. 2014). According to them, the modification of the FoF group finder was made to accommodate the finger-of-god effect on the radial distances to the SDSS DR10 galaxies. The group catalog of Tempel et al. (2014) provides various information on the properties of the member galaxies belonging to each group such as their galaxy identification number (ID), redshifts, equatorial positions, morphologies, absolute magnitudes, and so forth.

The morphological type of each member galaxy was obtained from the Galaxy Zoo Project of Lintott et al. (2008) and from the Bayesian analysis of Huertas-Company et al. (2011). The former classified the morphological types (T_z) of the galaxies as unclear ($T_z = 0$), spiral ($T_z = 1$) and elliptical ($T_z = 2$). Meanwhile, the latter estimated the four Bayesian probabilities, $P(E),\ P(S0),\ P(Sab),\ P(Scd)$, of each Sloan galaxy being

classified as an elliptical (E), lenticular (S0), early-type spiral (Sab), and late-type spiral (Scd), respectively.

From the FoF group catalog of Tempel et al. (2014), we search for the isolated spiral pairs which satisfy the following three conditions: (1) $n_g = 2$ where n_g is the number of the member galaxies constituting a FoF group; (2) $P_{\rm x} = P(Scd)$ or $P_{\rm x} = P(Sab)$ where $P_{\rm x} \equiv \max\{P(E),\ P(S0),\ P(Sab),\ P(Scd)\}$; (3) $T_z = 1$. An *isolated pair* means a FoF group composed of only two members without being embedded in any other larger FoF groups. From here on, the Sab galaxies refer to those spiral galaxies satisfying the conditions of $T_z = 1$ and $P_{\rm x} = P(Sab)$, while the Scd galaxies to those satisfying $T_z = 1$ and $P_{\rm x} = P(Sab)$.

We end up having a total of $3,021$ isolated spiral pairs from the FoF group catalog of Tempel et al. (2014). For each isolated spiral pair, we compare the absolute r-band magnitudes of its two members with each other and define a primary (secondary) member as the one with larger (smaller) values of $|M_r|$. The first two columns of Table 2.1 list the range of the redshifts and the absolute r-band magnitudes of the member galaxies in the isolated spiral pairs. Figure 2.1 shows the number distribution of the redshift difference, $|z_p - z_s|$ between the primary and the secondary members of the selected isolated spiral pairs. As can be seen, the majority of the pairs has $|z_p - z_s| \leq 0.001$.

As in Lee (2011), we adopt the *thin circular disk approximation* to estimate the directions of the spin angular momentum vectors of two members of each isolated spiral pair, which requires such information as the equatorial positions (RA and DEC), position angles (ψ_p), axial ratios (R_a) and morphological types of the member galaxies. Although the FoF group catalog of Tempel et al. (2014) does not contain information on ψ_p and R_a, we extract the values of ψ_p and R_a of each member galaxy from the web-site of the SDSS DR10[1] by matching the galaxy ID's.

[1] http://www.sdss3.org/dr10/

For the convenience of the readers, we briefly review the thin circular disk approximation: Let $\hat{\mathbf{J}}$ denote a unit vector in the direction of the spin axis of a member galaxy in a given isolated spiral pair. Expressing $\hat{\mathbf{J}}$ in the spherical polar coordinates such as $\hat{\mathbf{J}} = (\hat{J}_r, \hat{J}_\theta, \hat{J}_\phi)$, one can say that its radial component, $\hat{J}_r$, is the projection of $\hat{\mathbf{J}}$ onto the direction of the line-of-sight toward the spiral galaxy while its polar and azimuthal coordinates, $\hat{J}_\theta$ and $\hat{J}_\phi$, are the projection onto the plane orthogonal to the line of sight direction. Under the assumption that a spiral galaxy is a thin circular disk and its spin axis is perpendicular to the disk plane, the observed axial ratio, R_a, of a spiral galaxy should be the same as the cosine of the inclination angle, which is in turn equal to the *magnitude* of the radial coordinate of the spin vector: $R_a = \cos I_a \approx |\hat{J}_r|$ (see Pen et al. 2000, and references therein). Additional information on the position angle, ψ_p, of a spiral galaxy determines the other two coordinates: $\hat{J}_\theta = \sqrt{1 - \hat{J}_r^2}\sin\psi_p$ and $\hat{J}_\phi = \sqrt{1 - \hat{J}_r^2}\cos\psi_p$ (see Figure 2.2).

This simple routine based on the thin circular disk approximation for the determination of $\hat{\mathbf{J}}$ has two downsides. First, it is blind to the sign of the radial component $\hat{J}_r$ (Pen et al. 2000). Second, it's validity depends sensitively on the thinness of a disk. In other words, for a real spiral galaxy which usually have a central bulge, this routine is likely to fail. While the first weak point is a rather generic one that cannot be avoided, the second one may be overcome by making the following modification in the relation between I_a and R_a, as Haynes & Giovanelli (1984) suggested: $\hat{J}_r \cos^2 I_a \approx (R_a^2 - I_f^2)/(1 - I_f^2)$ where I_f is a *flatness parameter* introduced by Haynes & Giovanelli (1984) to account for the deviation of a spiral galaxy with a thick bulge from a thin disk. Following the suggestion of Haynes & Giovanelli (1984), we set the values of the flatness parameter at $I_f = 0.1$ and $I_f = 0.2$ for the Sab and Scd galaxies, respectively.

If the radial component of $\hat{\mathbf{J}}$ is positive, then the Cartesian coordinates, $\hat{\mathbf{J}} = (\hat{J}_x, \hat{J}_y, \hat{J}_z)$, of the unit spin vector of a spiral galaxy can now be written as (Pen

et al. 2000):

$$\hat{J}_{x+} = +\hat{J}_r \sin\theta\cos\phi + \hat{J}_\theta \cos\theta\cos\phi - \hat{J}_\phi \sin\phi\,, \tag{2.1}$$

$$\hat{J}_{y+} = +\hat{J}_r \sin\theta\sin\phi + \hat{J}_\theta \cos\theta\sin\phi + \hat{J}_\phi \cos\phi\,, \tag{2.2}$$

$$\hat{J}_{z+} = +\hat{J}_r \cos\theta - \hat{J}_\theta \sin\theta\,, \tag{2.3}$$

while, for the case of the negative radial component, the sign in front of $\hat{J}_r$ should be reversed as

$$\hat{J}_{x-} = -\hat{J}_r \sin\theta\cos\phi + \hat{J}_\theta \cos\theta\cos\phi - \hat{J}_\phi \sin\phi\,, \tag{2.4}$$

$$\hat{J}_{y-} = -\hat{J}_r \sin\theta\sin\phi + \hat{J}_\theta \cos\theta\sin\phi + \hat{J}_\phi \cos\phi\,, \tag{2.5}$$

$$\hat{J}_{z-} = -\hat{J}_r \cos\theta - \hat{J}_\theta \sin\theta\,. \tag{2.6}$$

The sign ambiguity in the determination of $\hat{\mathbf{J}}$ leads us to have four different realizations (say, $\alpha_1,\ \alpha_2,\ \alpha_3,\ \alpha_4$) of the alignment angles between the spin axes of the primary and the secondary member galaxies in each isolated spiral pair, as shown in Figure 2.3 (see discussions in Pen et al. 2000; Lee 2011):

$$\cos\alpha_1 = |\hat{\mathbf{J}}_{p+} \cdot \hat{\mathbf{J}}_{s+}|\,, \tag{2.7}$$

$$\cos\alpha_2 = |\hat{\mathbf{J}}_{p+} \cdot \hat{\mathbf{J}}_{s-}|\,, \tag{2.8}$$

$$\cos\alpha_3 = |\hat{\mathbf{J}}_{p-} \cdot \hat{\mathbf{J}}_{s+}|\,, \tag{2.9}$$

$$\cos\alpha_4 = |\hat{\mathbf{J}}_{p-} \cdot \hat{\mathbf{J}}_{s-}|\,. \tag{2.10}$$

From a total of N_{sp} isolated spiral pairs, we have $4N_{sp}$ realizations of $\cos\alpha$.

Partitioning the range of $[0,\ 1]$ into five small intervals each of which has an equal length of $\Delta\cos\alpha = 0.2$, we calculate $p(\cos\alpha_i)$ at each interval of $[\cos\alpha_i, \cos\alpha_i + \Delta\cos\alpha_i]$ as $p(\cos\alpha_i) = n_{i,sp}/(\Delta\cos\alpha \cdot N_{sp})$, where $n_{i,sp}$ denotes the number of the realizations

of $\cos\alpha$ belonging to the ith interval of $\cos\alpha$. Figure 2.4 displays as filled circles the probability density function of the cosines of the angles of the isolated spiral pairs, $p(\cos\alpha)$, from the flux-limited samples of the SDSS DR10. If there were no alignment between the spin vectors of the two members in the isolated spiral pairs, then the expectation of the probability density function would be constant as $p(\cos\alpha) = 1$ (dotted line). As shown, the observational results deviate significantly from the constant distribution, revealing that the directions of the spin axes of the primary and the secondary members in the isolated spiral pairs are not random but preferentially aligned with each other.

Generating $10,000$ Bootstrap resamples from the original sample of the isolated spiral pairs, the uncertainty σ_i involved in the measurement of $p(\cos\alpha_i)$ at the ith $\cos\alpha$-interval is calculated as one standard deviation scatter averaged over the $10,000$ resamples:

$$\sigma_i^2 = \frac{1}{N_{boot}} \sum_{k=1}^{N_{boot}} \left[p^k(\cos\alpha_i) - p(\cos\alpha_i) \right]^2 , \tag{2.11}$$

where $p^k(\cos\alpha_i)$ is the probability density function from the kth Bootstrap resample and N_{boot} is the numbers of the Bootstrap resamples.

To see if the strength of the intrinsic spin alignment depends on the morphological types of the spiral galaxies, we divide the isolated spiral pairs into three different subsamples: Sab-Sab, Scd-Scd and Sab-Scd pairs. The first (second) subsample consists only of two early-type (two late-type) galaxies, while the third sample contains those pairs consisting of one Sab and one Scd galaxies. For each of the three subsamples, we redo all of the calculations described in the above. The numbers of the Sab-Sab, Sab-Scd and Scd-Scd pairs are listed in the last three columns of Table 2.1, respectively. Figure 2.5, 2.6, 2.7 show $p(\cos\alpha)$ versus α as filled circles for the three cases of the Sab-Sab, Sab-Scd and Scd-Scd pairs, respectively. As shown, the Sab-Sab pairs exhibit a clear signal of intrinsic spin alignment, while no statistically significant signals are

found from the Sab-Scd nor from the Scd-Scd pairs. For the case of the Sab-Scd pairs, the probability density function $p(\cos\alpha)$ shows an abrupt drop at the fourth bin from the left. We suspect that this odd behavior might be caused by some unknown systematics involved in the determination of the directions of the spin axes of the member galaxies.

To quantitatively assess the statistical significance of the alignment signals detected from the isolated spiral pairs, we employ the Kolmogorov-Smirnov (KS) method and test the null hypothesis that the spin vectors in the isolated spiral pairs are random relative to each other. Figure 2.12 and 2.13 show the cumulative probability distributions, $P(>\cos\alpha) \equiv \sum p(\cos\alpha)\Delta\cos\alpha$, (solid lines) for the cases of all spiral and Sab-Sab pairs, respectively. In each figure, the cumulative uniform distribution $P_u(>\cos\alpha) = \cos\alpha$ (dotted lines) is compared with $P(>\cos\alpha)$ and the maximum distance between $P(>\cos\alpha)$ and $\cos\alpha$ is marked as red arrow. With the help of the KS test, we find that the confidence levels at which the null hypothesis is rejected reach as high as 99.99% and 100% for the cases of all spiral and Sab-Sab pairs, respectively.

Although the KS test is quite reliable, it is subject to an idealistic assumption that the values of $p(\cos\alpha)$ at the five $\cos\alpha$-intervals are mutually independent. In reality, any systematics in our measurements of the alignment angles could cause spurious correlations between the values of $p(\cos\alpha)$ at two adjacent $\cos\alpha$-intervals. Concerning about the existence of this possible correlations, we also calculate the generalized chi-squared as

$$\chi^2 = \sum_{i=1}^{5} \left[p(\cos\alpha_i) - 1\right] C_{ij} \left[p(\cos\alpha_j) - 1\right] , \tag{2.12}$$

where the covariance matrix $\mathbf{C} = (C_{ij})$ is calculated from the Bootstrap resamples as

$$C_{ij} = \frac{1}{N_{boot}} \sum_{k=1}^{N_{boot}} \left[p^k(\cos\alpha_i) - p(\cos\alpha_i)\right] \left[p^k(\cos\alpha_j) - p(\cos\alpha_j)\right] . \tag{2.13}$$

The subtraction of unity from $p^k(\cos\alpha_i)$ in Equation (2.13) is in accordance with the

fact that the null hypothesis predicts $\langle p(\cos\alpha_i)\rangle = 1$ at each $\cos\alpha$-interval. This generalized chi-squared statistics yield slightly reduced confidence levels of 99.99% and 98.37% at which the null hypothesis is rejected for the cases of all spiral and Sab- Sab pairs, respectively.

We investigate the dependence of the strength of intrinsic spin alignments on the luminosity ratios by calculating $\langle\cos\alpha\rangle$ as a function of $10^{(M_{r,s}-M_{r,p})/2.5}$, where $M_{r,p}$ and $M_{r,s}$ denote the r-band absolute magnitudes of the primary and secondary galaxies in each isolated spiral pairs, respectively. Dividing the whole range $10^{(M_{r,s}-M_{r,p})/2.5}$ into several short intervals of equal length, we evaluate the mean value of $\cos\alpha$ averaged over those pairs whose luminosity ratios lie in the range of a given interval. The results are shown in Figure 2.14 and 2.15 for the cases of all spiral and Sab-Sab pairs, respectively. As can be seen, for both of the cases, the alignment signals tend to be stronger as the luminosity ratios are closer to unity (i.e., $10^{(M_{r,s}-M_{r,p})/2.5} \approx 1$). This result implies that those isolated spiral pairs with members having more comparable masses yield stronger signals of spin alignments.

The dependence of the strength of intrinsic alignment on the angular separation distances between the primary and the secondary galaxies in the isolated spiral pairs is also investigated in a similar manner by measuring $\langle\cos\alpha\rangle$ versus the angular separation distance, φ, which can be readily calculated from the equatorial coordinates of the member galaxies:

$$\cos\varphi = \cos(\mathrm{Dec}_p)\cos(\mathrm{Dec}_s) - \sin(\mathrm{Dec}_p)\sin(\mathrm{Dec}_s)\cos(\mathrm{RA}_p - \mathrm{RA}_s)\,, \qquad (2.14)$$

where $\{\mathrm{Dec}_p,\ \mathrm{RA}_p\}$ ($\{\mathrm{Dec}_s,\ \mathrm{RA}_s\}$) is the equatorial coordinates of the primary (secondary) members in each isolated spiral pair. Note that this 2D projected distance between the two members in each isolated spiral pair can be obtained without specifying the background cosmology. Figure 2.16 and 2.17 show $\langle\cos\alpha\rangle$ versus φ for the cases of all spiral and Sab-Sab pairs, respectively. As can be seen, the intrinsic spin align-

ments in the isolated spiral pairs show a mild tendency to increase with the decrement of the angular separation distances: The more closely located the member galaxies are, the more strongly their spin axes are aligned with each other.

Table 2.1. Isolated spiral pairs in the flux-limited sample.

Redshift	M_r	N_{Sab}	N_{Scd}	N_{Sm}
[0.0104, 0.1983]	[−22.77, −16.02]	1129	523	1369

Note. — In both tables, Sab indicates early-type(Sab-Sab) pairs, Scd indicates late-type(Scd-Scd) pairs, and Sm indicates mixed-type(Sab-Scd) pairs.

Table 2.2. Isolated spiral pairs in the volume-limited sample.

Sample	Redshift	M_r	N_{Sab}	N_{Scd}	N_{Sm}
V1	[0.0104, 0.0457]	[−22.17, −17.99]	82	124	222
V2	[0.0111, 0.0570]	[−22.17, −18.48]	143	161	338
V3	[0.0111, 0.0718]	[−22.17, −19.00]	261	165	442
V4	[0.0111, 0.0890]	[−22.26, −19.50]	467	175	583
V5	[0.0111, 0.1105]	[−22.53, −19.82]	505	130	501
V6	[0.0143, 0.1372]	[−22.53, −20.49]	405	69	370
V7	[0.0299, 0.1679]	[−22.77, −20.97]	119	28	117

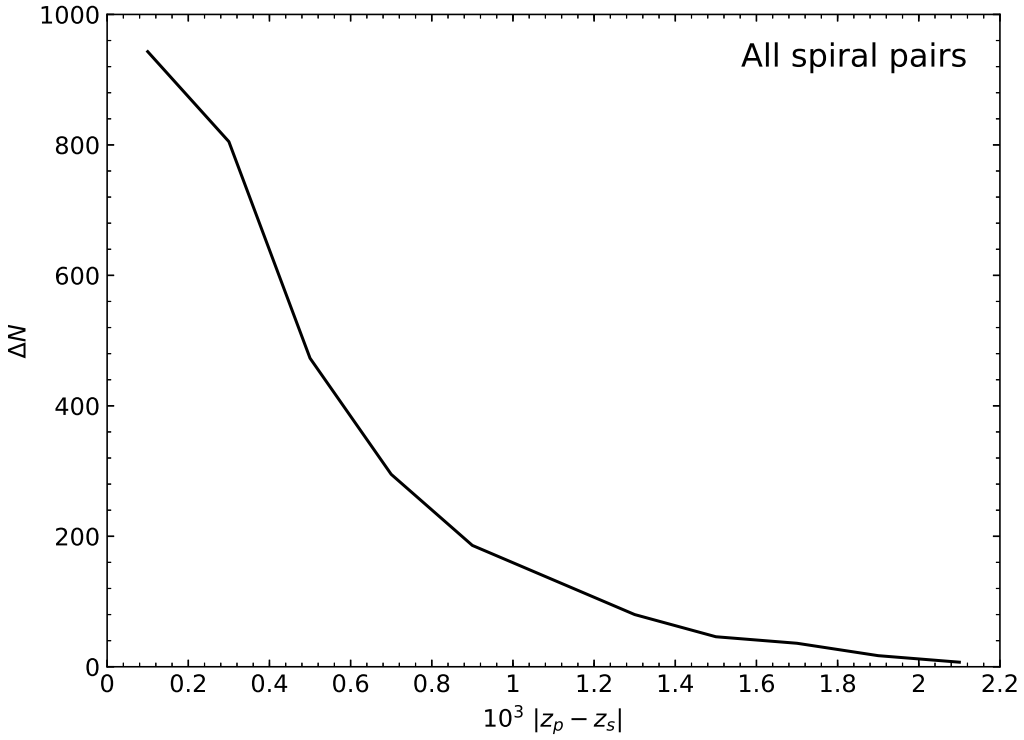

Figure 2.1 Distributions of the numbers of the isolated spiral pairs versus the differences between the redshifts of the primary and the secondary member galaxies.

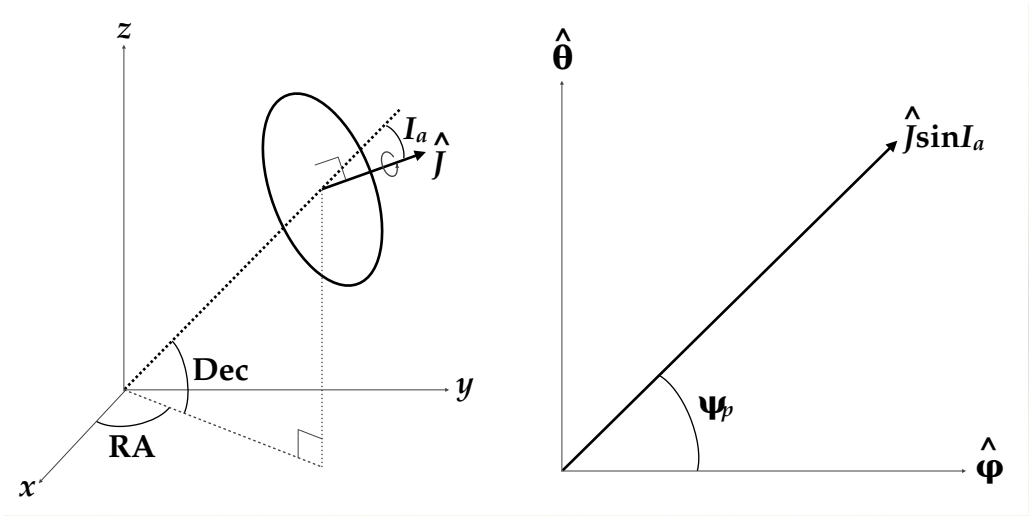

Figure 2.2 Configuration of the spin angular momentum vector of a thin circular disk-like spiral galaxy in the equatorial coordinate system.

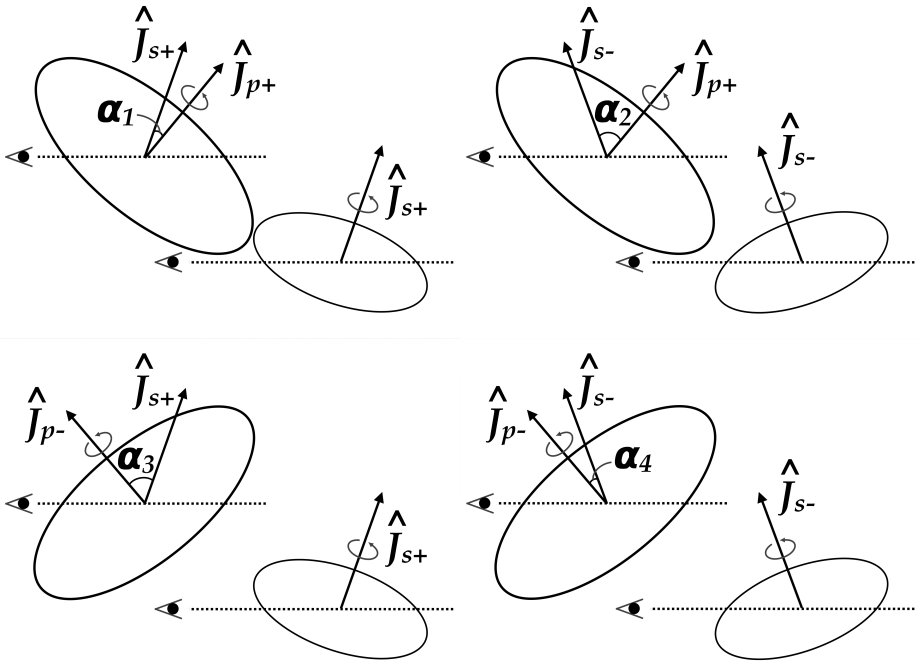

Figure 2.3 Illustration of the four-fold degeneracy involved with the measurement of the cosine of the alignment angles between the spin axes of the member galaxies in a spiral pair.

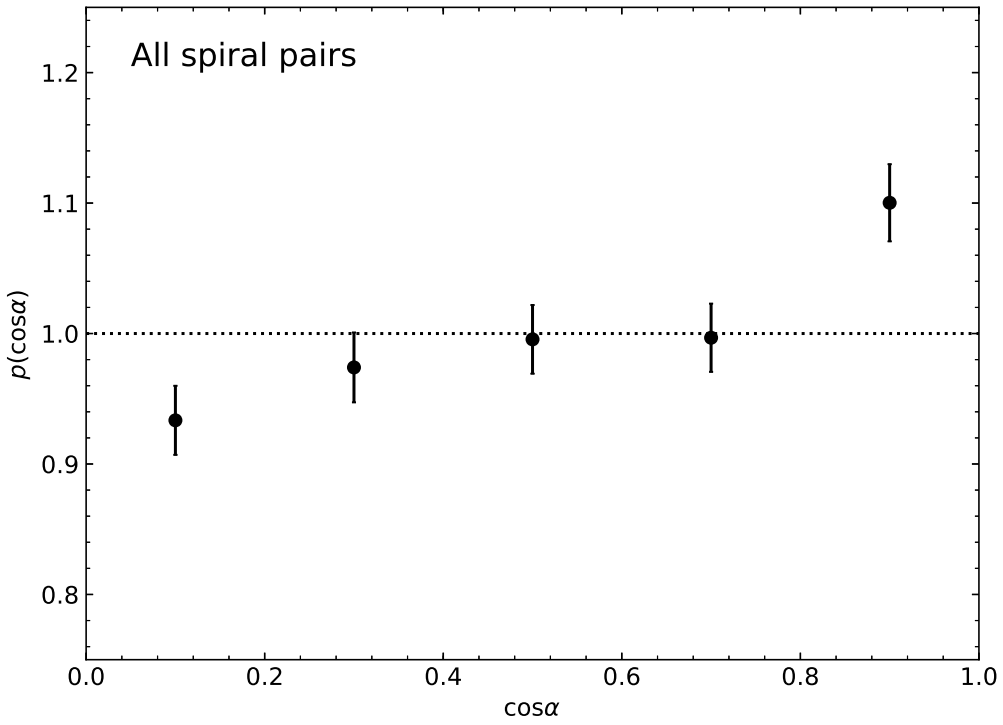

Figure 2.4 Probability density functions of the cosines of the angles between the spin axes of the members in the isolated all types spiral pairs from the SDSS DR10. The dotted line displays a uniform distribution.

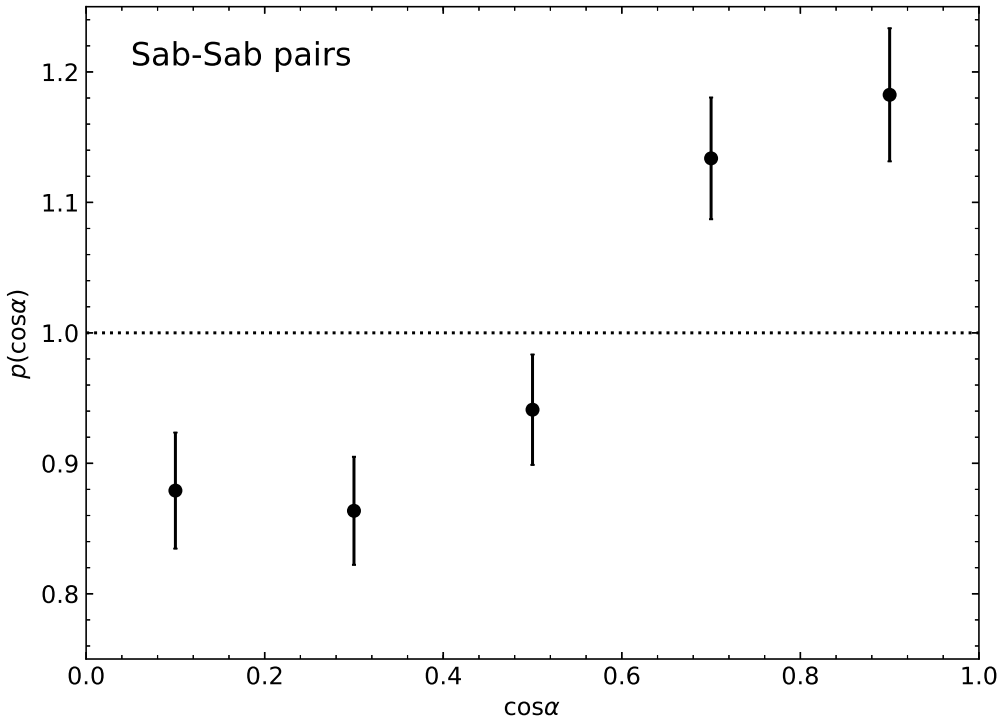

Figure 2.5 Same as Figure 2.4 but for early-type(Sab-Sab) spiral pairs.

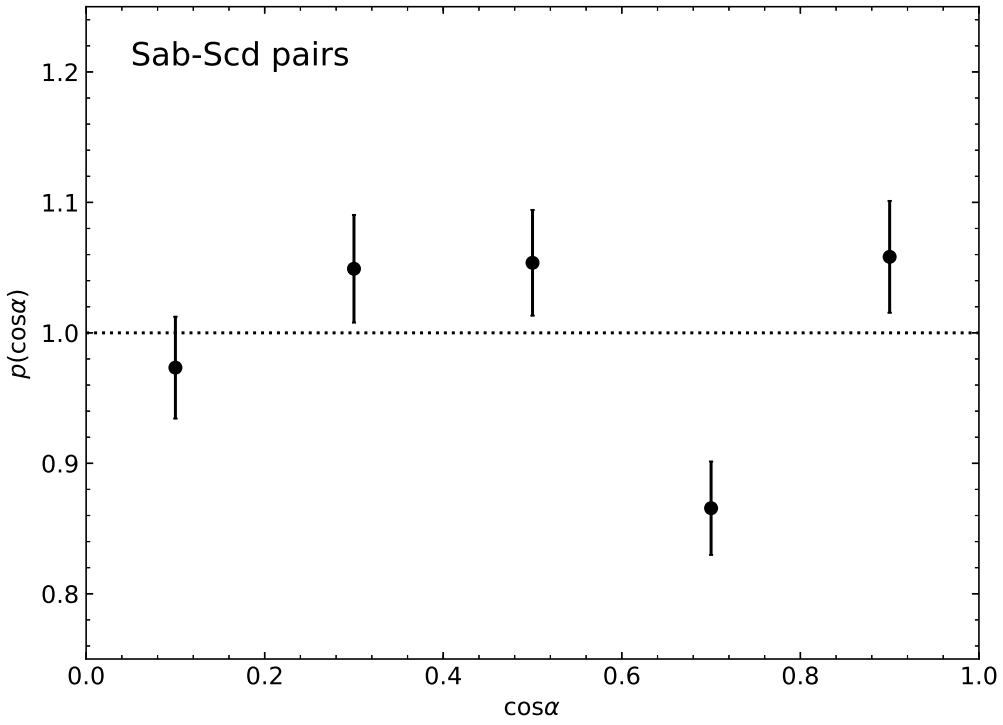

Figure 2.6 Same as Figure 2.4 but for mixed-type(Sab-Scd) spiral pairs.

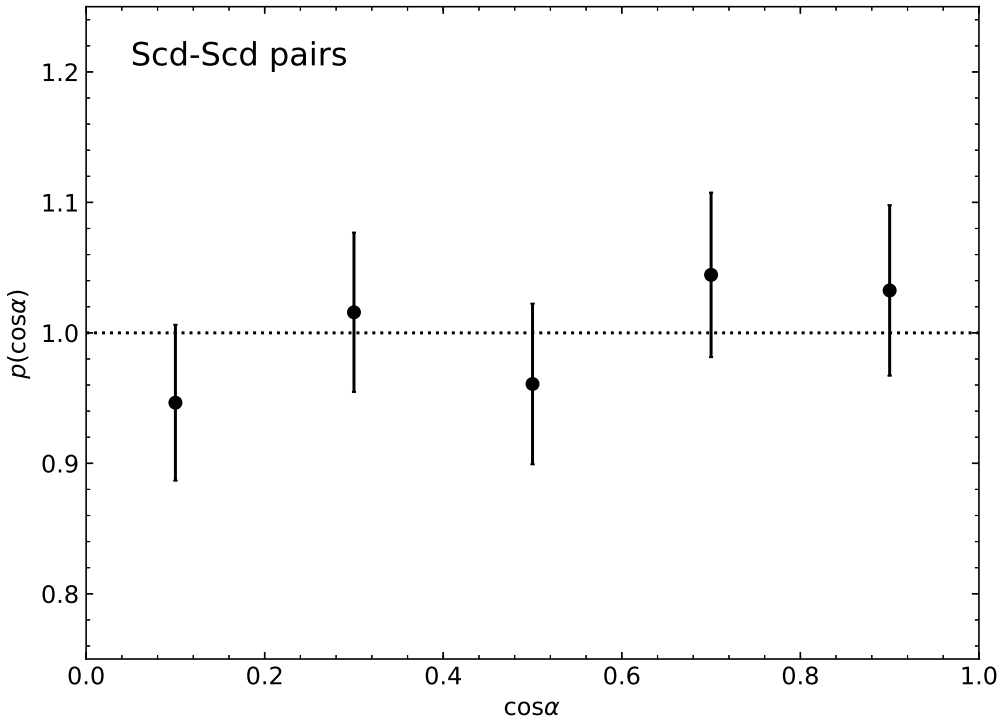

Figure 2.7 Same as Figure 2.4 but for late-type(Scd-Scd) spiral pairs.

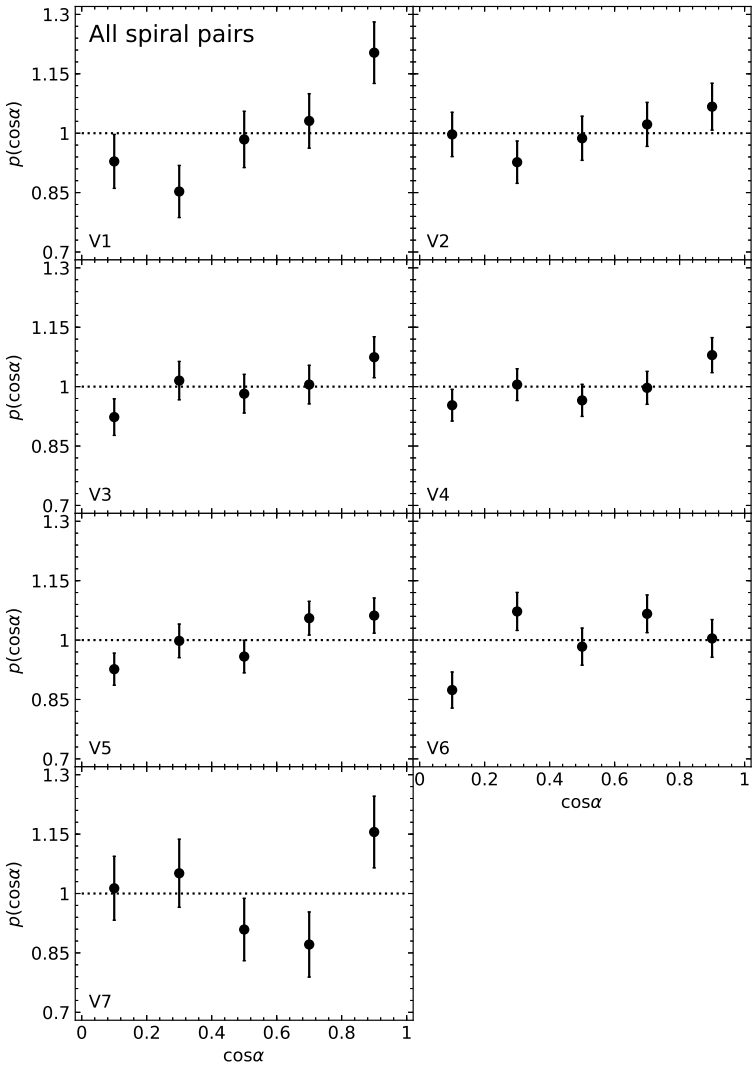

Figure 2.8 Probability density functions of the cosines of the angles between the spin axes of the members in the volume-limited samples of isolated all types spiral pairs from the SDSS DR10. The dotted line displays a uniform distribution.

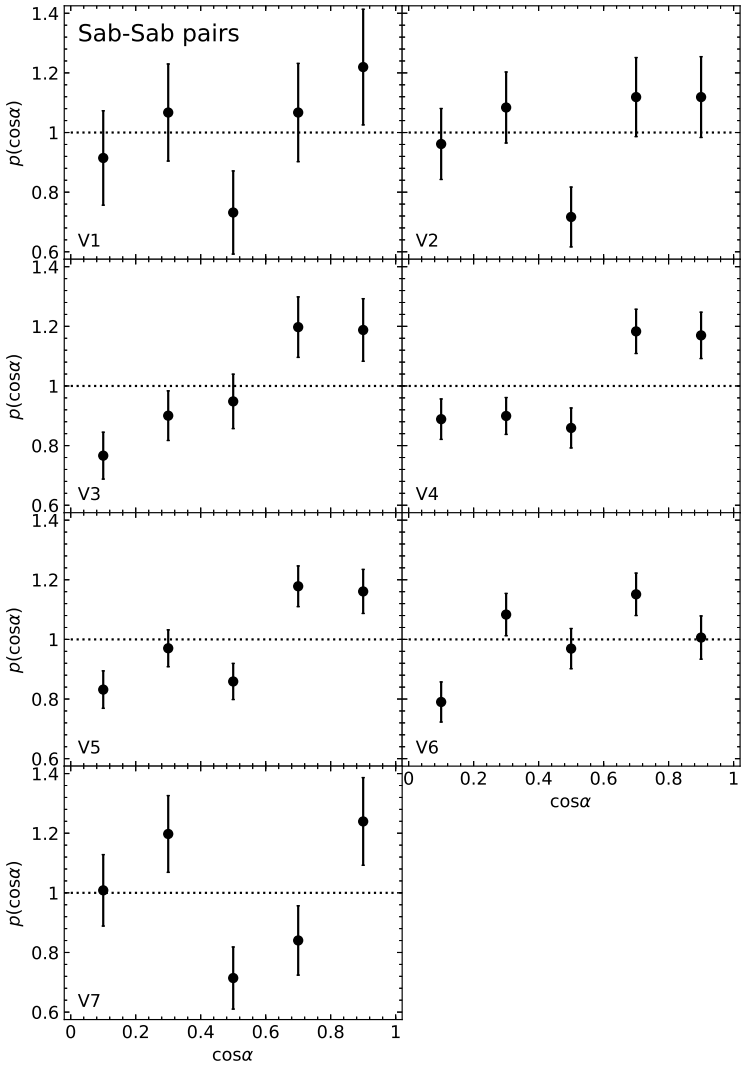

Figure 2.9 Same as Figure 2.8 but for early-type(Sab-Sab) spiral pairs.

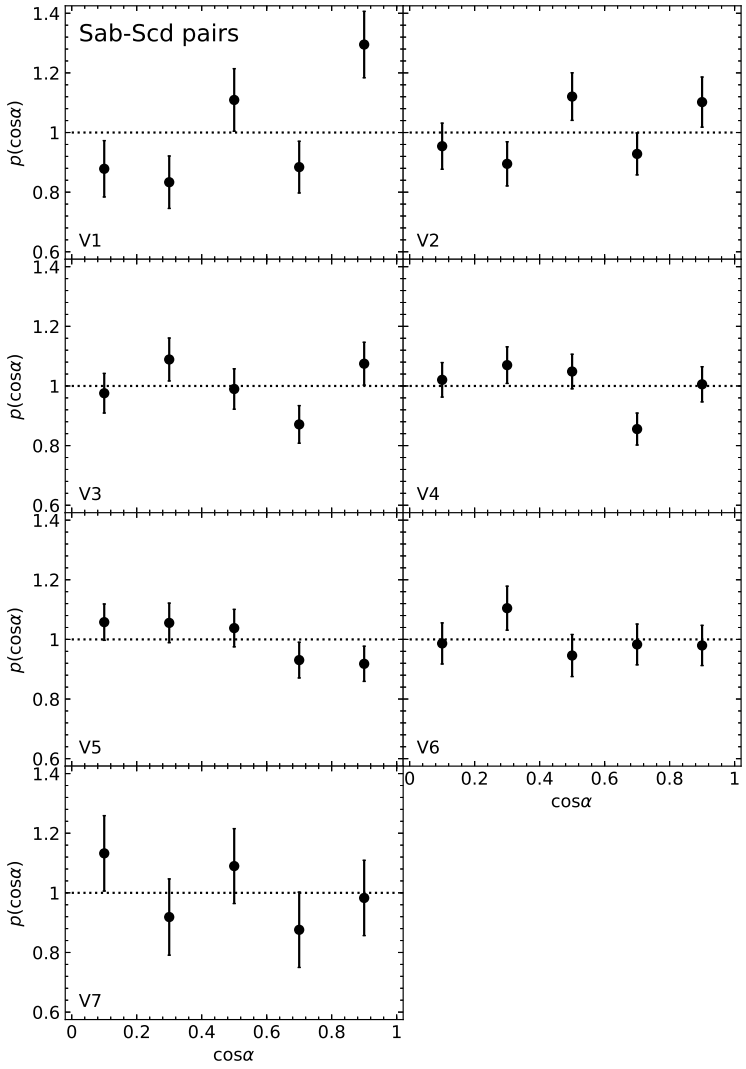

Figure 2.10 Same as Figure 2.8 but for mixed-type(Sab-Scd) spiral pairs.

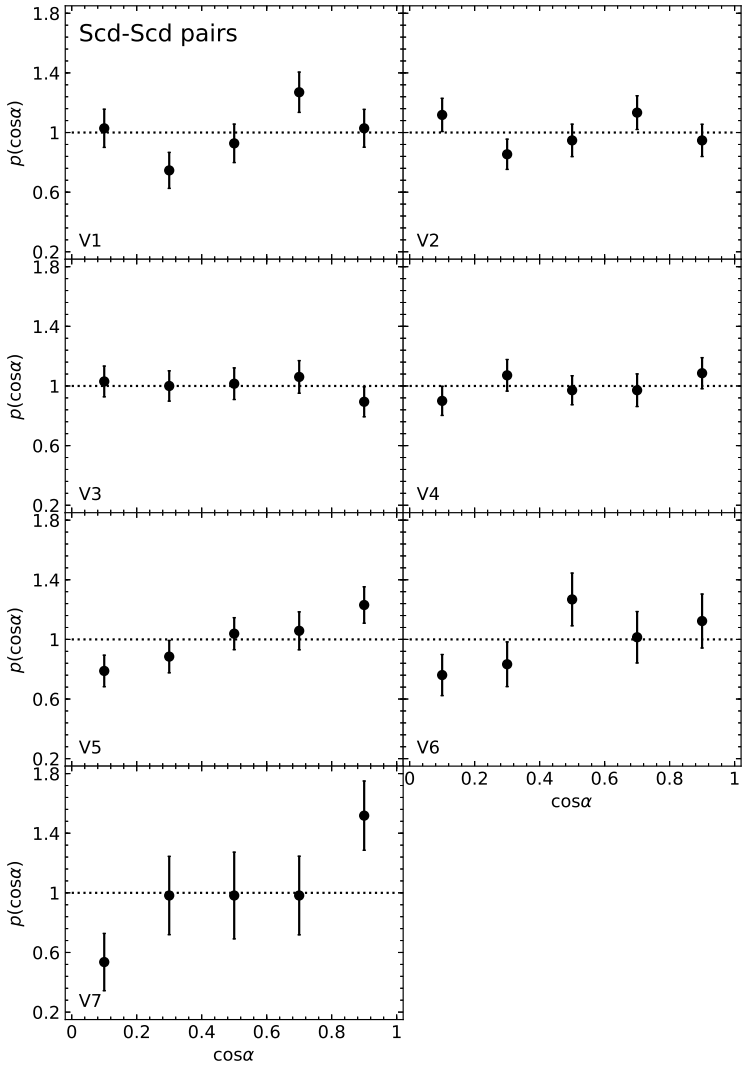

Figure 2.11 Same as Figure 2.8 but for late-type(Scd-Scd) spiral pairs.

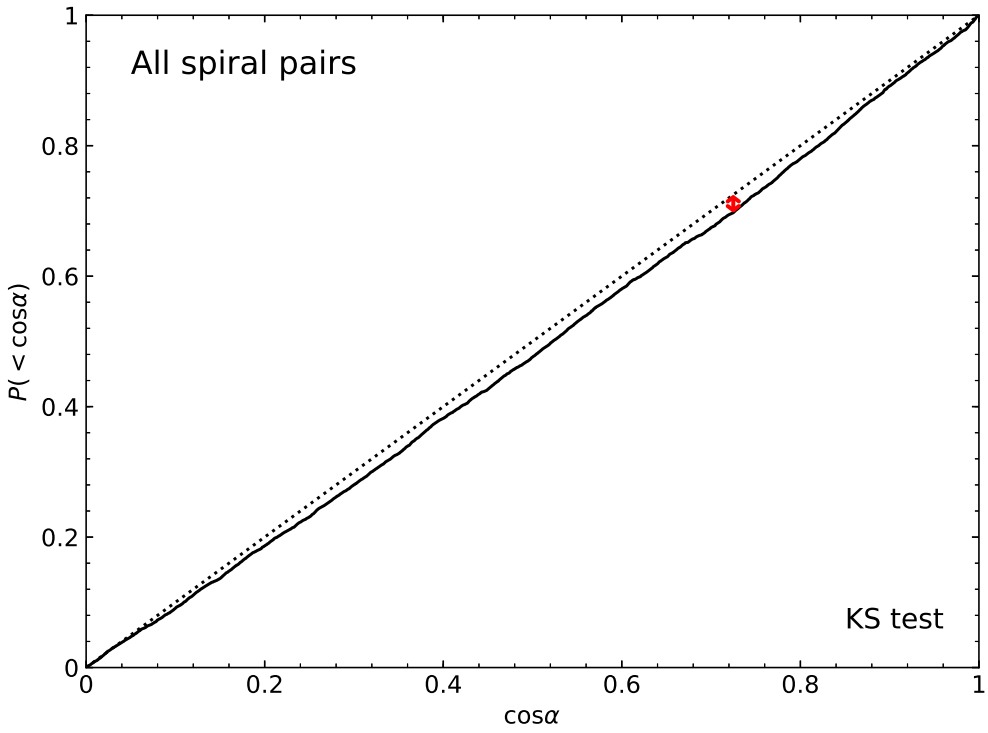

Figure 2.12 Cumulative probability distributions of $\cos\alpha$ to perform the KS tests of the null hypothesis. The solid and dotted lines represent the observational results from the SDSS DR10 and the theoretical predictions based on the null hypothesis, respectively. The arrow corresponds to the maximum distance between the observational result and the theoretical prediction.

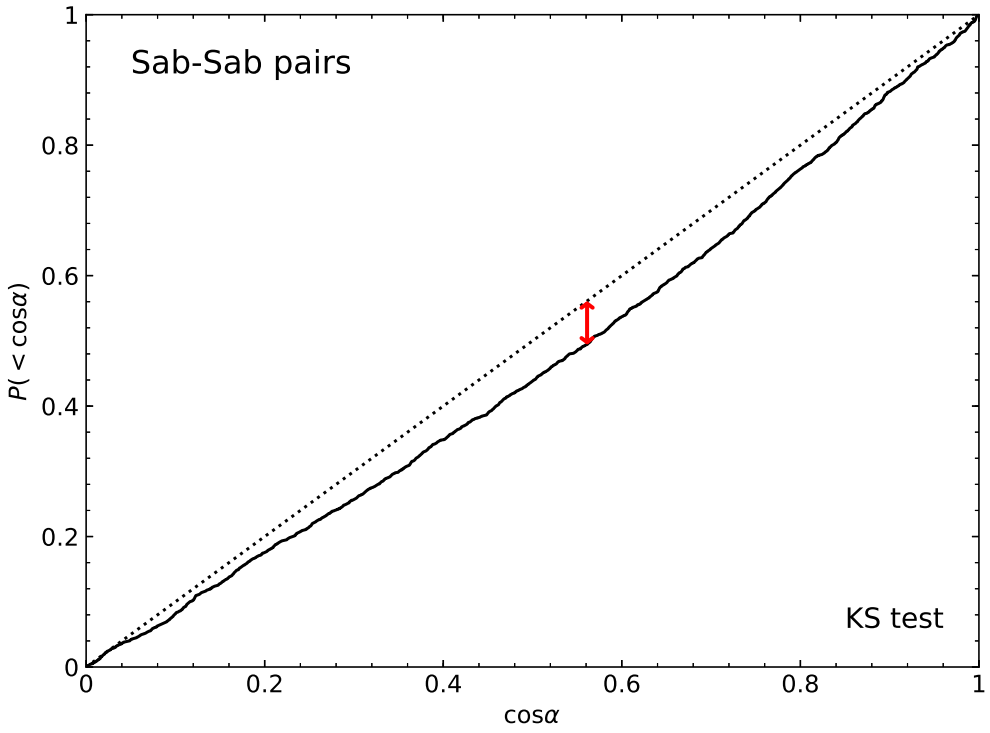

Figure 2.13 Same as Figure 2.12 but for early-type(Sab-Sab) spiral pairs.

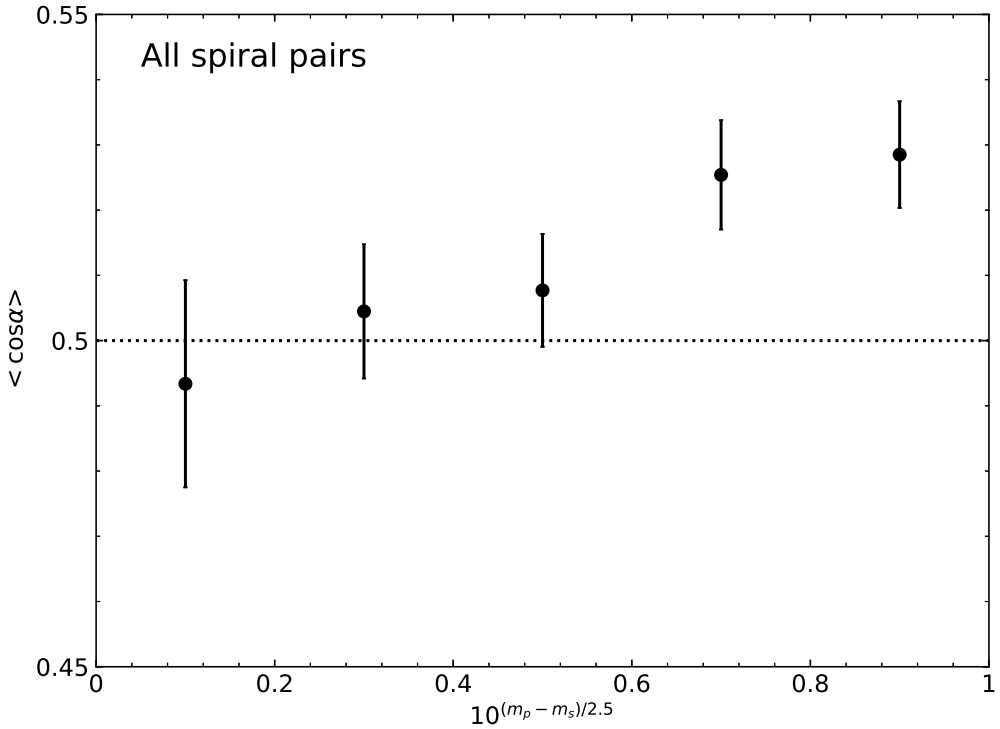

Figure 2.14 Mean values of the cosines of the alignments angles versus the r-band luminosity ratios of the member galaxies in the isolated spiral pairs.

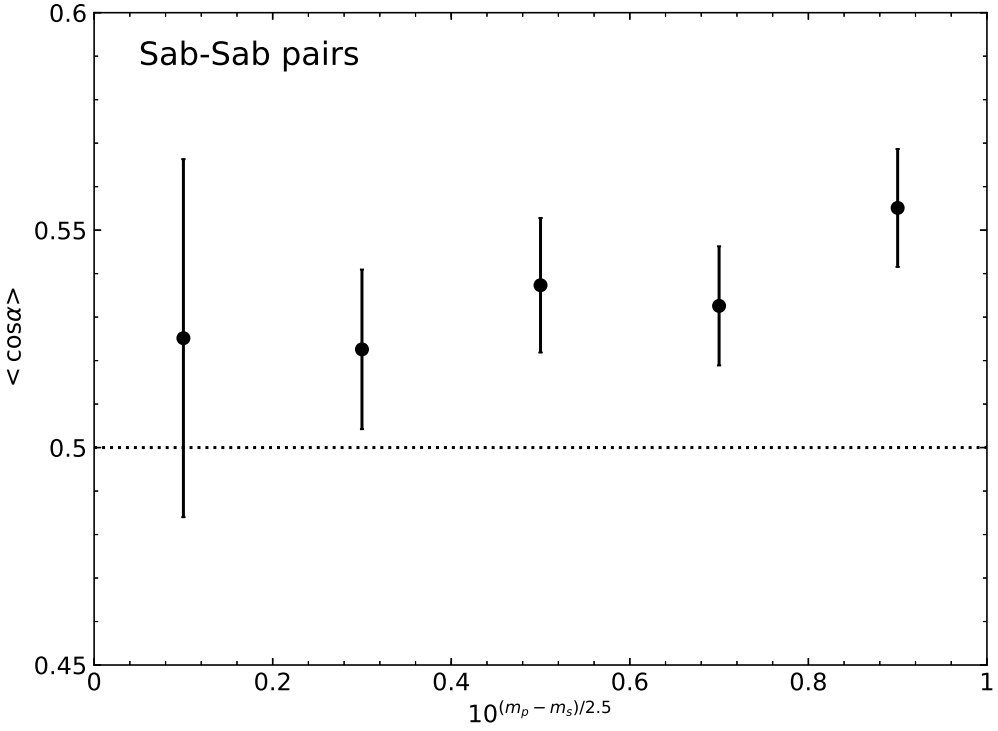

Figure 2.15 Same as Figure 2.14 but for early-type(Sab-Sab) spiral pairs.

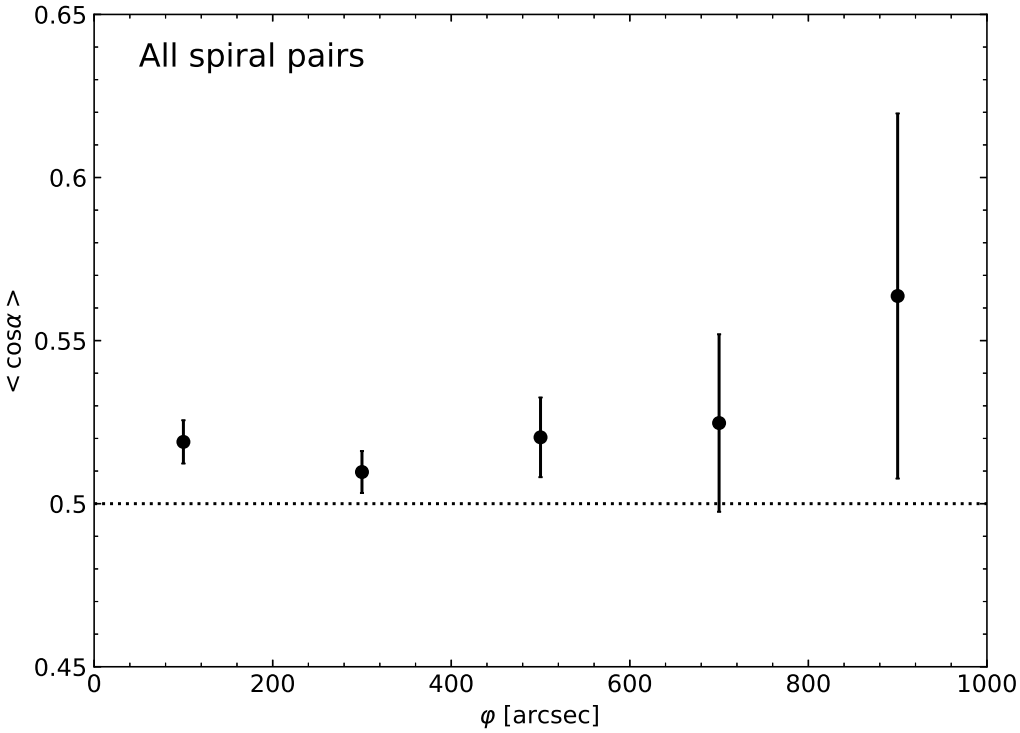

Figure 2.16 Mean values of the cosines of the alignments angles versus the angular separation distance between the member galaxies in the isolated spiral pairs.

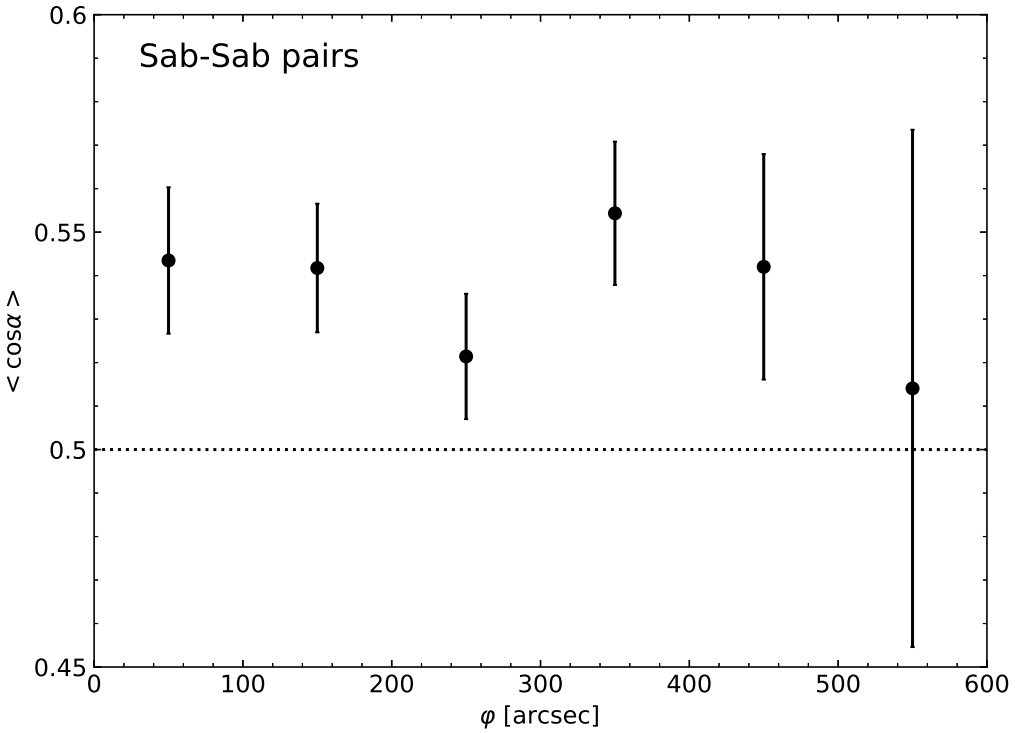

Figure 2.17 Same as Figure 2.16 but for early-type(Sab-Sab) spiral pairs.

Chapter 3

Numerical Predictions of the ΛCDM Cosmology

To compare the observational results obtained in Section 2 with the theoretical predictions of the ΛCDM cosmology, we utilized the data from the EAGLE project of cosmological hydrodynamic simulations that were run on a periodic box of 100 comoving mega parsecs (cMpc) with a total of 2×1504^3 dark matter particles (Crain et al. 2015; McAlpine et al. 2016; Schaye et al. 2015). Assuming a ΛCDM universe with initial conditions constrained by the angular power spectrum of the temperature fluctuation field of the Microwave Background (CMB) measured by the Planck survey (Planck Collaboration et al. XVI 2014a), the EAGLE project computed the influences of various baryonic processes as well as gravity to simulate the realistic evolutions of the luminous galaxies that reside in the DM halos. (Schaye et al. 2015). The standard FoF group finder and the SUBFIND algorithms (Springel et al. 2001; McAlpine et al. 2016) were used by the EAGLE project to find DM halos and to resolve the subhalos within the virial radius of each DM halo, respectively. From the website of the EAGLE hydrodynamic simulations[1], one can access the catalogs of the FoF groups and their

[1] http://icc.dur.ac.uk/Eagle/database.php

subhalos at various redshifts from $z = 127$ to $z = 0$ and extract such information as the spin angular momentum vectors, position vectors and virial masses of the subhalos.

We consider two different redshifts, $z = 0$ and 0.1, to match the redshift ranges of the isolated spiral pairs analyzed in Section 2 (see Table 2.1). Analyzing the DM halo and subhalo catalogs at each redshift, we search for those DM halos which have only two subhalos and define them as the isolated pair systems. Table 3.1 lists the numbers of the isolates pair systems as well as the mass ranges of the primary and the secondary subhalos at two different redshifts. Here, a primary (secondary) subhalo refers to the one with higher (lower) virial mass in each isolated pair system.

Each subhalo carries three different angular momentum vectors: One from the DM particles, another from the gas particles, and the third from their stellar components. Since the spin axes of the observed spiral galaxies we have determined in Section 3 are the angular momentum vectors of the stellar components but not of the DM nor of the gas particles, we use the third ones to measure the intrinsic spin alignments in the isolated pair systems.

For each isolated pair system at each redshift, we compute the cosine of the angle between the angular momentum vectors of the stellar components of the two subhalos. Unlike the case of the observed spiral galaxies, there is no ambiguity in the directions of the spin angular momentum of the stellar components of the subhalos. Therefore each isolated halo system yields only one value of the cosine of the alignment angle. Repeating the same procedures described in Section 2, we determine the probability density functions of the cosines of the alignment angles between the angular momentum vectors of the stellar components of the subhalos in the isolated halo systems at $z = 0$ and 0.1, which are plotted in Figure 3.1 and 3.2. As can be seen, the distributions $p(\cos\alpha)$ at both of the redshifts show almost no change over $[0,\ 1]$, indicating no signal of intrinsic spin alignment in the isolated pair system from the EAGLE simulations based on the ΛCDM cosmology.

To find an answer to the question if a signal of intrinsic spin alignment can be found from those pair systems with two subhalos having comparable masses, we calculate $\langle \cos \alpha \rangle$ as a function of the ratio of the mass of a primary subhalo to that of a secondary subhalo, M_s/M_p, and show the results in Figure 3.3 and 3.4. No correlation is found between $\langle \cos \alpha \rangle$ and M_s/M_p, which leads us to conclude that even for those pair systems composed of two subhalos with comparable masses the directions of their spin axes are randomly oriented relative to each other.

To see if a signal of intrinsic spin alignment can be found from those pair systems where two subhalos are more closely located to each other than the average, we calculate $\langle \cos \alpha \rangle$ as a function of the 3D separation (comoving) distances between the subhalos and show the results in Figure 3.5 and 3.6. As can be seen, the average of the cosines of the alignment angles does not show any sign of increment with the decrement of the separation distance, indicating that no matter how closely located the two subhalos are, their spin axes are not aligned.

In fact, the galaxy catalog from the EAGLE project was already used by Velliscig et al. (2015) to investigate the galaxy intrinsic alignments. However, what they examined is not the intrinsic spin alignments in the isolate pair systems but the alignments between the halo shapes and the alignments between the halo shapes and the cosmic web.

Table 3.1. Isolated pairs in the EAGLE simulation.

Redshift	M_p $(10^8\,h^{-1}M_\odot)$	M_s $(10^8\,h^{-1}M_\odot)$	N_{pair}
0	$[3.51,\ 2.97\times10^3]$	$[1.54,\ 3.98\times10^2]$	2606
0.1	$[5.39,\ 2.74\times10^3]$	$[1.60,\ 3.01\times10^2]$	2866

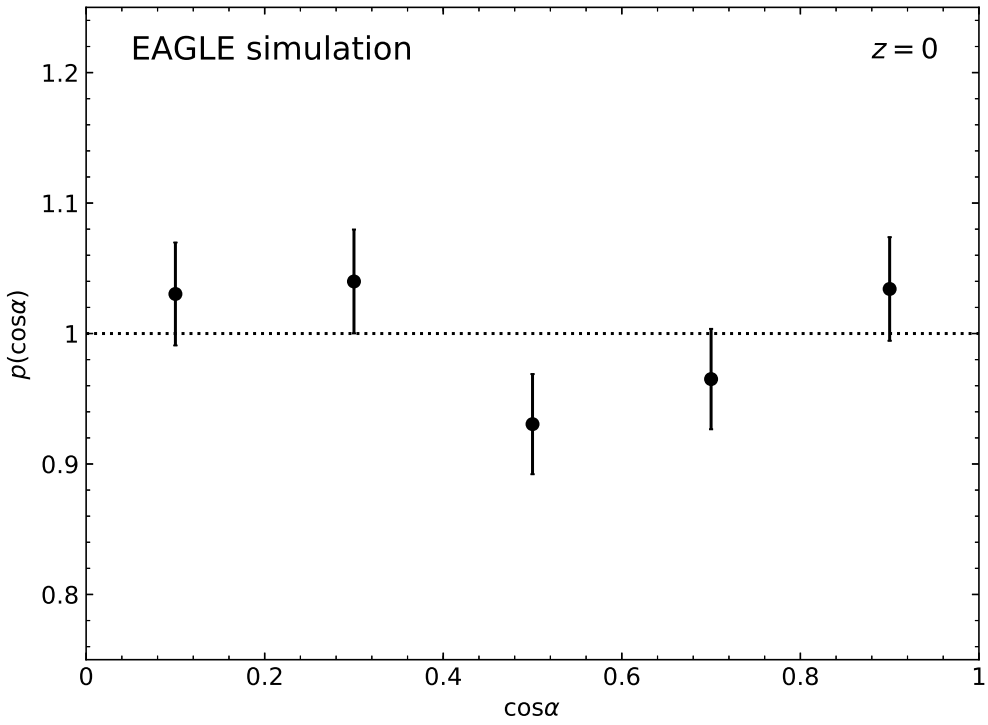

Figure 3.1 Probability density functions of the cosines of the alignment angles between the spin vectors of the stellar parts of the subhalos in the isolated pairs from the Eagle cosmological hydrodynamic simulation at $z = 0$.

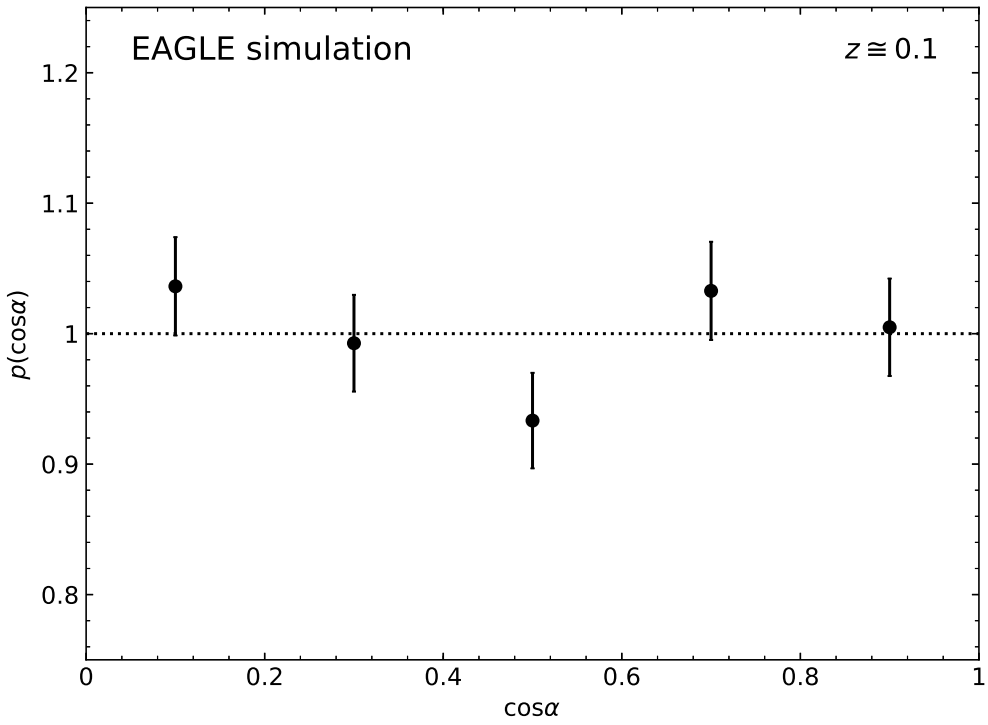

Figure 3.2 Same as Figure 3.1 but from the EAGLE simulation at $z \cong 0.1$

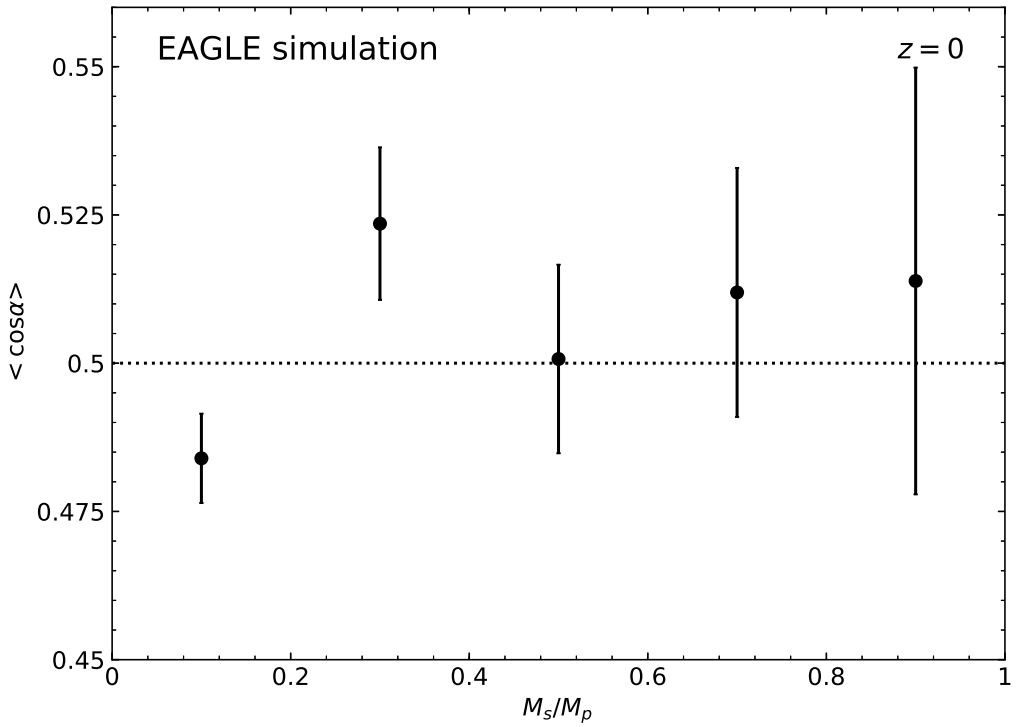

Figure 3.3 Mean values of the cosines of the alignments angles versus the ratios of the masses of the secondary subhalos to those of the primary ones in the isolated pair systems from the EAGLE simulation at $z = 0$.

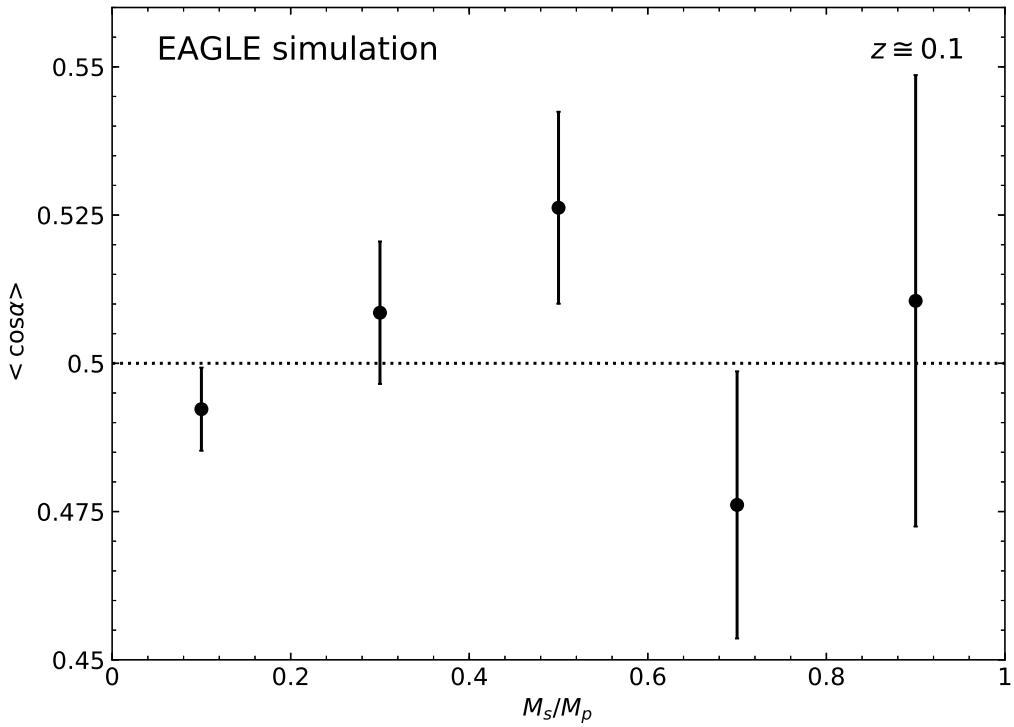

Figure 3.4 Same as Figure 3.3 but from the EAGLE simulation at $z \cong 0.1$.

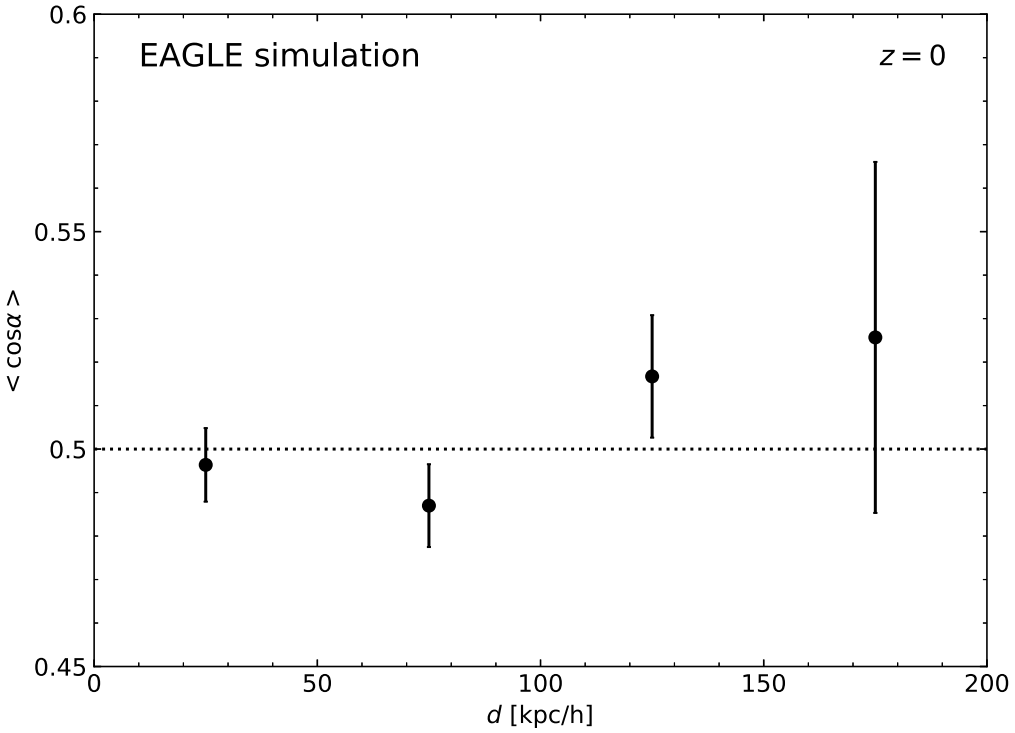

Figure 3.5 Mean values of the cosines of the alignments angles versus the 3D distances between the member subhalos in the isolated pair systems from the EAGLE simulation at $z = 0$.

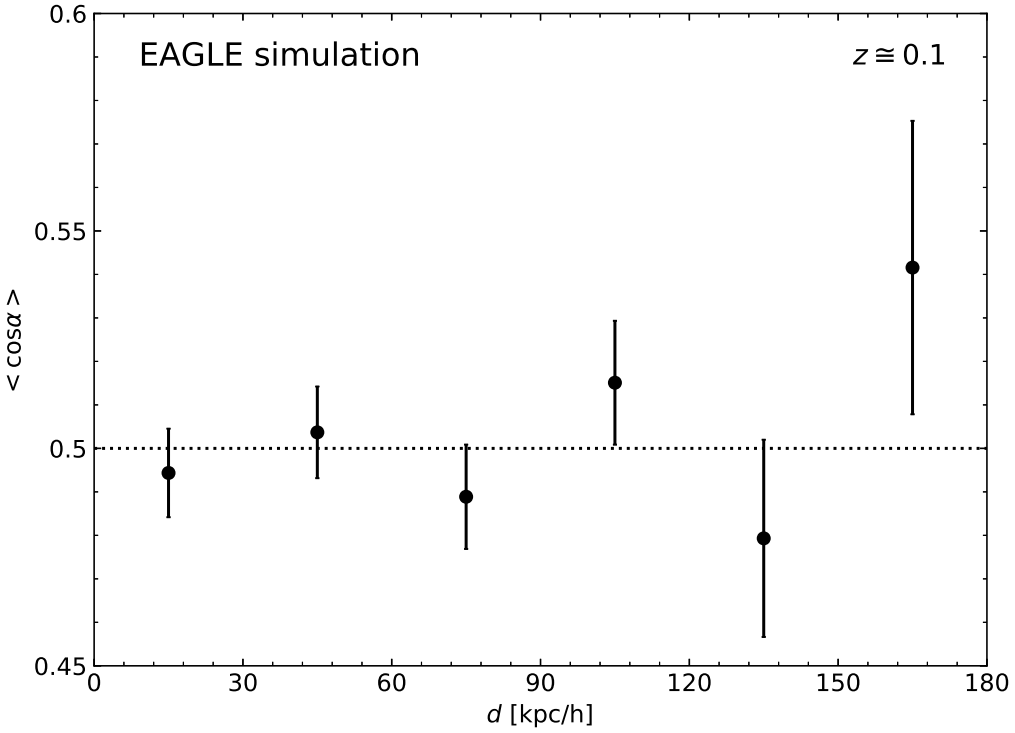

Figure 3.6 Same as Figure 3.5 but from the EAGLE simulation at $z \cong 0.1$.

Chapter 4

Summary and Discussion

We have investigated whether or not the 3D spin vectors of the member galaxies belonging to the isolated spiral pairs are aligned with each other by utilizing the FoF group catalog of the SDSS DR10 galaxies (Ahn et al. 2014; Tempel et al. 2014). Defining the isolated spiral pairs as the FoF groups composed of only two spiral (Sab or Scd) galaxies without being embedded in any other larger FoF groups, we have detected a clear signal of intrinsic spin alignment between the directions of the 3D spin axes of the two member galaxies. The generalized chi squared and the KS tests have rejected the null hypothesis of no signal at the 99.99% and 98.37% confidence levels, respectively. The strength of the alignment signal has been found to depend on the morphological types and the luminosity ratios of the member galaxies as well as their separation distances. The Sab-Sab pairs produce the strongest signal, while the weakest signal has been found in the Sab-Scd pairs. Those isolated spiral pairs whose member galaxies are more closely located to each other with comparable l uminosities have been also shown to yield a stronger alignment tendency.

To see whether or not the detected signal of intrinsic spin alignment in the isolated spiral pairs can be naturally explained by the ΛCDM cosmology, we have also conducted a similar investigation with the data from the EAGLE cosmological hydro-

dynamic simulations (Schaye et al. 2015; McAlpine et al. 2016). Selecting the isolated dark matter halos consisting of only two subhalos from the EAGLE cosmological hydrodynamic simulations, we have determined the alignment angles between the spin angular momentum vectors of the stellar parts of two subhalos in each pair but eventually failed to find no signal of intrinsic spin alignments. This result agrees well with the previous one obtained by Lee (2012) who found no signal of alignments between the angular momentum vectors of the subhalos in the isolated FoF groups from the H-CoDECS (Baldi 2012). Recalling that in Lee (2012) the angular momentum vectors of the subhalos were calculated not from the stellar parts but from the DM particles that constitute the subhalos, the agreement between the two results implies that for a ΛCDM cosmology there is no gravitational nor hydrodynamical mechanism that can create the alignments between the spin vectors of the subhalos in the isolated pairs.

As the tension between the observational and the numerical results calls for a physical explanation, we suggest three possible scenarios. The first scenario concerns about the inaccuracy in the measurements of the directions of the spin axes of the spiral galaxies from the SDSS DR10. Since the shapes of real spiral galaxies are not perfectly circular nor infinitesimally thin, the directions of their spin axes determined under the circular thin disk approximation may be inaccurate enough to produce a spurious signal of intrinsic alignment. It may be not only the thin circular disk approximation but also any other uncertainties associated with the determination of the morphological types and the flatness parameter for the spiral galaxies that might have produced a false signal of intrinsic spin alignments in the isolated spiral pairs.

Besides, there is a notable difference between the observational and the numerical analyses. For the former, we have considered only the spiral galaxies, excluding the lenticular and ellipticals, simply because the circular thin disk approximation is not applicable to the excluded ones. For the numerical analysis, however, we considered all isolated pair systems without making any discrimination according to the morpholog-

ical of the galaxies. This difference might be responsible partly for the inconsistency between the observational and the numerical results on the intrinsic spin alignments in the isolated pairs. To answer the question of how the exclusion of the elliptical and lenticulars would affect the strength of alignment signal, it will be necessary either to develop a method with which the directions of the spin vectors of the elliptical and lenticulars are determined or to use a more elaborate hydrodynamical simulation which is capable of distinguishing among spiral, lenticular and elliptical galaxies.

The second scenario ascribes the inconsistency to some missing baryon process that was not included in the EAGLE hydrodynamic simulations. Although the spin vectors of the DM components of the subhalos in the isolated pair systems are not aligned with each other as shown by Lee (2012), some unknown baryon processes might be able to generate alignments between the spin vectors of the stellar counterparts. If this process were incorporated into a hydrodynamical simulation, then the simulation would yield an alignment signal as strong as the detected one from observations. It will be, however, a daunting task to figure out what that missing baryon process should be.

The third scenario is the most radical one, claiming that the observed signal of intrinsic spin alignments should be a new local anomaly that challenges the ΛCDM model on the small-scale. The spin alignments in the isolated spiral pairs can be produced if the member galaxies interact strongly with each other after they form a bound pair and reside in a dynamically isolated state (Gott & Thuan 1978; Helou 1984; Lee 2012). This scenario basically interprets the numerical results from the EAGLE and H-CoDECS simulations as an indication that in a ΛCDM cosmology the mutual interaction between the subhalos do not occur efficiently enough to produce the intrinsic alignments, and claims that in the cDE models the fifth force produced by the dark sector coupling could stimulate the interactions between the member galaxies in the isolated pairs, generating the intrinsic spin alignments (Lee 2012). In this scenario, the stronger signal of intrinsic spin alignment detected from the Sab-Sab pairs may be also

explained with the same logic: Since the Sab-Sab galaxies are expected to have formed earlier than the Scd-Scd and Scd-Sab pairs, their members must have interacted for a longer period of time during which stronger spin alignments are induced. Radical as this third scenario may sound, it would be less difficult to test than the first two, requiring only a hydrodynamical simulation for a cDE cosmology. Our future work is in this direction.

Bibliography

Adermann, E., Elahi, P. J., Lewis, G. F., & Power, C. 2017, MNRAS, 468, 3381

Ahn, C. P., Alexandroff, R., Allende Prieto, C., et al. 2014, ApJS, 211, 17

Amendola, L., & Tsujikawa, S. 2010, Dark Energy : Theory and Observations, Cambridge University Press, ISBN: 9780521516006,

Baldi, M., Pettorino, V., Robbers, G., & Springel, V. 2010, MNRAS, 403, 1684

Baldi, M. 2012, MNRAS, 422, 1028

Barnes, J., & Efstathiou, G. 1987, ApJ, 319, 575

Bland-Hawthorn, J., & Peebles, P. J. E. 2006, Science, 313, 311

Catelan, P., & Theuns, T. 1996, MNRAS, 282, 436

Carlesi, E., Mota, D. F., & Winther, H. A. 2017, MNRAS, 466, 4813

Cervantes-Sodi, B., Hernandez, X., & Park, C. 2010, MNRAS, 402, 1807

Codis, S., Pichon, C., Devriendt, J., et al. 2012, MNRAS, 427, 3320

Crain, R. A., Schaye, J., Bower, R. G., et al. 2015, MNRAS, 450, 1937

Doroshkevich, A. G. 1970, Astrofizika, 6, 581

Dubinski, J. 1992, ApJ, 401, 441

Gott, J. R., III, & Thuan, T. X. 1978, ApJ, 223, 426

Hahn, O., Teyssier, R., & Carollo, C. M. 2010, MNRAS, 405, 274

Haynes, M. P., & Giovanelli, R. 1984, AJ, 89, 758

Helou, G. 1984, ApJ, 284, 471

Huertas-Company, M., Aguerri, J. A. L., Bernardi, M., Mei, S., & Sánchez Almeida, J. 2011, A&A, 525, A157

Huterer, D., Shafer, D. L., Scolnic, D. M., & Schmidt, F. 2017, JCAP, 5, 015

Koo, H., & Lee, J. 2017, [arXiv:1707.03549]

Lee, J., & Pen, U.-L. 2000, ApJ, 532, L5

Lee, J., & Pen, U.-L. 2001, ApJ, 555, 106

Lee, J., & Erdogdu, P. 2007, ApJ, 671, 1248

Lee, J. 2011, ApJ, 732, 99

Lee, J. 2012, ApJ, 751, 153

Linder, E. V. 2005, Phys. Rev. D, 72, 043529

Lintott, C. J., Schawinski, K., Slosar, A., et al. 2008, MNRAS, 389, 1179

McAlpine, S., Helly, J. C., Schaller, M., et al. 2016, Astronomy and Computing, 15, 72

Nielsen, J. T., Guffanti, A., & Sarkar, S. 2016, Scientific Reports, 6, 35596

Oosterloo, T. 1993, A&A, 272, 389

Pavlidou, V., & Tomaras, T. N. 2014, JCAP, 9, 020

Peebles, P. J. E. 1969, ApJ, 155, 393

Peebles, P. J. E. 2017, arXiv:1705.10683

Pen, U.-L., Lee, J., & Seljak, U. 2000, ApJ, 543, L107

Perlmutter, S., Aldering, G., Goldhaber, G., et al. 1999, ApJ, 517, 565

Pestaña, J. L. G., & Cabrera, J. 2004, MNRAS, 353, 1197

Planck Collaboration, Ade, P. A. R., Aghanim, N., et al. 2014, A&A, 571, A16

Planck Collaboration, Ade, P. A. R., Aghanim, N., et al. 2014, A&A, 571, A20

Porciani, C., Dekel, A., & Hoffman, Y. 2002, MNRAS, 332, 325

Riess, A. G., Filippenko, A. V., Challis, P., et al. 1998, AJ, 116, 1009

Schaye, J., Crain, R. A., Bower, R. G., et al. 2015, MNRAS, 446, 521

Sharp, N. A., Lin, D. N. C., & White, S. D. M. 1979, MNRAS, 187, 287

Springel, V., White, S. D. M., Tormen, G., & Kauffmann, G. 2001, MNRAS, 328, 726

Tempel, E., Tamm, A., Gramann, M., et al. 2014, A&A, 566, A1

Tenneti, A., Gnedin, N. Y., & Feng, Y. 2017, ApJ, 834, 169

Velliscig, M. et al. 2015, MNRAS, 454, 3328

White, S. D. M. 1984, ApJ, 286, 38

Zhao, G.-B., Li, B., & Koyama, K. 2011, Physical Review Letters, 107, 071303

Zjupa, J., & Springel, V. 2017, MNRAS, 466, 1625

요 약

본 논문에서는 다수의 고립된 나선 은하쌍에서 보이는 은하 간의 고유한 정렬을 보여주는 관측 증거를 다룬다. Tempel et al.에서 Sloan Digital Sky Survey Data Release 10에 포함된 은하 중에 은하군을 구별하여 카탈로그를 만들었고, 본 논문에서는 이 중에서 2개의 나선 은하로만 구성된 은하군을 고립된 은하쌍으로 구별하고, 구별한 은하쌍 내의 두 은하의 스핀 회전축이 얼마나 강하게 정렬되어 있는지 분석한다. 그리하여 고립된 나선 은하쌍의 고유한 스핀 정렬에서 4σ signal을 발견했고, 이는 Kolmogorov-Smirnov test를 통해 계산한 귀무 가설이 부정될 가능성이 99.999%인 경우에 해당한다. 또한 고립된 은하쌍이 조기형 나선 은하로만 구성된 경우에 가장 강한 고유 스핀 정렬을 보이는 것을 발견했고, 반면에 후기형 나선 은하로만 구성된 경우에는 가장 약한 정렬을 보이는 것을 발견했다. 뿐만 아니라 강하게 정렬된 정도가 은하쌍 사이의 각거리 및 은하쌍 간의 광도 비율과 상관관계가 있는 것을 발견했다. EAGLE 유체역학적 시뮬레이션에서 2개의 subhalo로만 구성된 암흑 물질 halo를 구별하여 같은 분석을 했으나 두 subhalo의 항성으로 구성된 부분 간의 스핀 정렬을 발견하지 못했고, 이는 관측 자료로 분석한 결과와 충돌한다. 근거리 우주에서 발견된 이 변칙 사례의 몇 가지 가능성 있는 원인을 본 논문에서 논의한다.

주요어: 우주론:이론 — 우주 거대 구조

학 번: 2014 – 21385